ACS OMEGA

Article

http://pubs.acs.org/journal/acsodf

Preferential Mitochondrial Localization of a Goniothalamin Fluorescent Derivative

Ismael Raitz,[†] Roberto Y. de Souza Filho,[§] Lorena P. de Andrade,[§] Jose R. Correa,[*,∥] Brenno A. D. Neto,[*,§] and Ronaldo A. Pilli[*,†,‡]

[†]Institute of Chemistry, University of Campinas, Cidade Universitária Zeferino Vaz, 13083-970 Campinas, SP, Brazil

[‡]Obesity and Comorbidities Research Center, University of Campinas, Cidade Universitária Zeferino Vaz, 13083-862 Campinas, SP, Brazil

[§]Laboratory of Medicinal and Technological Chemistry, Institute of Chemistry, University of Brasília, Campus Universitário Darcy Ribeiro, 70904-970 Brasília, DF, Brazil

[∥]Laboratory of Microscopy and Microanalysis, Institute of Biological Sciences, University of Brasília, Campus Universitário Darcy Ribeiro, 70910-900 Brasília, DF, Brazil

Supporting Information

ABSTRACT: A fluorescent 2,1,3-benzothiadiazole-containing goniothalamin derivative, BTD−GTN (**1**), has been synthesized and successfully tested in bioimaging experiments in live cells. The fluorescent compound proved to be capable of transposing the cell membranes, indicating its subcellular localization. The use of the benzothiadiazole core as the fluorophore revealed the favored localization of the GTN analogue **1** in the cytoplasm of live cells, preferentially in the mitochondria, in line with previous results that indicated the loss of mitochondrial transmembrane potential upon treatment with GTN. The results described herein highlight the potential of the BTD−GTN hybrid structures for future studies regarding the cellular mechanism of action of this family of compounds.

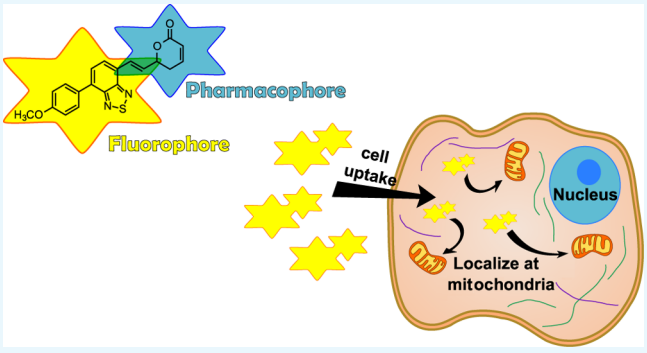

INTRODUCTION

Goniothalamin (GTN) is a styryl lactone isolated from genus *Goniothalamus* (*Annonaceae*), which despite its structural simplicity has shown promising antiproliferative and cytotoxic activities against several tumor cell types.[1] These effects have also been observed for several of its derivatives.[2,3] GTN is a low-molecular-weight secondary metabolite, which can be prepared through a straightforward synthetic procedure, and, so far, in our in vivo studies, it did not display systemic acute toxicity in the effective doses, therefore qualifying itself as a promising candidate for preclinical studies. Previous studies performed by our group have shown that racemic GTN presents gastroprotective effects and anti-inflammatory activity and inhibits the development of Ehrlich tumor in mice.[4−6] Recently, we have also shown that GTN prevents the development of prostate cancer in TRAMP mice as well as induces apoptosis in HT-29 colon tumor cells, which were dependent on reactive oxygen species (ROS) generation and caspase activation.[7,8]

The current understanding of its biological role points toward its involvement in the cell redox balance due to the electrophilic nature of the unsaturated δ-lactone and its influence on apoptotic pathways, with some authors favoring the mitochondrial membrane potential impairing and disbalance on the concentration of the oxidizing species.[9−11]

Our previous studies concerning the biochemical pathways influenced by the action of the natural form of GTN and its enantiomer in the human kidney cell line (786-0) showed that both compounds caused apoptosis in renal cancer cells. Although differences in the expression of some biochemical markers were found in this study, results indicated that both compounds were involved in the apoptosis and autophagy processes, albeit in different degrees.[11] Additionally, we have shown that the racemic form of GTN exhibits the same antiproliferative profile as natural GTN when a panel of nine cancer cell lines were evaluated. Moreover, in vivo results have shown that there is no statistically significant difference for the antiproliferative action of both enantiomers as well as between them and the racemic form of GTN when an Ehrlich solid tumor model was employed.[4]

Despite several in vivo studies indicating the antiproliferative and anti-inflammatory activities of GTN and derivatives,[3,6] the

Received: April 6, 2017
Accepted: June 28, 2017
Published: July 20, 2017

DOI: 10.1021/acsomega.7b00416
ACS Omega 2017, 2, 3774−3784

cellular localization of GTN and its derivatives remains uncertain, preventing a better comprehension of the cellular processes involved and the rational design of more effective analogues for further studies.

Fluorescent probes are powerful tools in cell and chemical biology and have contributed to our growing understanding of biological systems, enabling us the visualization of events with a temporal and spatial resolution. 2,1,3-Benzothiadiazole (BTD) derivatives are widely used in photochemical and photophysical studies.[12] Early works have proved that π-extended BTDs are also a promising class of fluorescent heterocycles applied for live-cell-imaging experiments.[13] Some of us have recently highlighted the beneficial features of using fluorescent BTD derivatives for bioimaging experiments.[14] Their capacity of transposing the cell membrane, excellent signal-to-noise ratios, bright emission with no notable blinking of the naked eye, and good chemical stability and photostability in both ground and excited states are fostering the interest of other research groups on the use of new fluorescent derivatives incorporating the BTD core for different purposes of cell-imaging studies.[15−17] Important organelles and cell components, such as nuclear DNA, mitochondria, lipid droplets, and others, have already been successfully labeled by fluorescent BTD molecules.[14]

The strategy of using fluorescent tags to gain insights into the subcellular localization and mechanisms of action of bioactive compounds typically returns attractive results and points to some preferential cellular pathways. For instance, the cellular uptake in pancreatic tumor cells was evaluated with a high-affinity receptor ligand (PB28) tagged with fluorescent dansyl, indicating that it may undergo endocytic paths.[18] Subcellular labile iron pools, which are still poorly understood, were evaluated using a new rhodamine-tagged ferric complex, revealing that they were preferentially localized within both endosomes and lysosomes in HeLa cells.[19] Human mesenchymal stem cells proved to internalize fluorescent thiophene-tagged compounds, allowing their subcellular localization.[20] Recently, some of us have tested a fluorescent oleic acid tagged with a BTD core to study the active internalization process and dynamics in live cells at 4 °C (complete endocytic pathway inhibition), depicting the preferential concentration in lipid droplets.[21]

BTDs may also be used as fluorescent tags to disclose the cellular dynamics and the mechanism of action of bioactive compounds. Although it is true that the incorporation of a fluorescent tag may change the biological response of a bioactive compound, this elegant strategy has been successfully used in several studies.[22,23]

In this context, we hypothesized that a hybrid structure containing the structural motifs of GTN and BTD would be valuable to study the cellular uptake and localization in live cells of this promising class of styryl lactones. Figure 1 shows the structure of the planned fluorescent GTN derivative, namely, BTD−GTN (**1**), bearing an electron-donating group (4-MeOPh) attached to the BTD core, which is known to be a strong electron acceptor heterocyclic,[12] to facilitate an intramolecular charge transfer (ICT) stabilizing process and a conjugation of the BTD core to the dihydropyran-2-one motif (GTN core) with the BTD core, emulating the aromatic ring present in GTN.

Due to our continuing interest in the biological application of BTD derivatives[12−14] and our ongoing research in the assessment of the cytotoxic properties of GTN and related derivatives,[2−8] we describe herein the synthesis, photophysical properties, and cell-imaging experiments of a new BTD hybrid structure, namely, BTD−GTN (**1**).

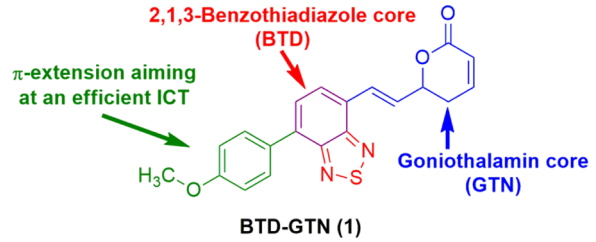

Figure 1. Fluorescent GTN derivative BTD−GTN (**1**) bearing a BTD core used in the current study.

RESULTS AND DISCUSSION

The synthesis of the racemic form of BTD−GTN hybrid structure **1** was performed following our previously described methodology for the synthesis of GTN (Scheme 1).[3] The conversion of commercially available aldehyde **2** to the corresponding unsaturated ester **3** via the Horner−Wadsworth−Emmons reaction paved the way for its Suzuki coupling with 4-methoxyphenyl boronic acid in 85% yield. Ester **4** was then converted to BTD-aldehyde **5**, which underwent allylation under standard Grignard conditions to afford homoallylic alcohol **6**. After esterification with acryloyl chloride and ring-closing metathesis reaction with Grubbs II catalyst, the desired BTD−GTN hybrid **1** was isolated as a fluorescent yellow solid, in 11% overall yield from aldehyde **2**, and characterized by UV−vis, fluorescence emission, ^{1}H NMR, and ^{13}C NMR spectroscopies and electrospray ionization (ESI)−high-resolution mass spectrometry (HRMS) (see Supporting Information).

BTD−GTN (**1**) had its photophysical properties evaluated in different solvents, and the results are summarized in Table 1 and Figure 2.

Large Stokes shifts (ranging from 104 to 152 nm) and molar extinction coefficients (log ε values in the range of 3.94−4.00 mM^{-1} cm^{-1}) are noted for BTD−GTN (**1**). These results indicate a clear ICT stabilizing process from the excited state. The lowest energy absorption bands are assigned to characteristic $\pi-\pi^*$ transitions typical from conjugated BTD derivatives.[24] On the basis of the data from Table 1, we could describe the solvent effect in the first excited state using the microscopic solvent polarity parameters (E_T^N) in the solvatochromic method,[25] applying values provided by Reichardt.[26] Without considering water, the R^2 value obtained from the plot is 0.80, therefore in accordance with an efficient ICT from the first excited state.

BTD−GTN (**1**) proved to be a very stable structure even under direct and constant irradiation in aqueous media (405, 366, and 254 nm) for 120 min (Figure S1). This important feature points to efficient bioimaging experiments without blinking or fading off (noted by the naked eye), as it is expected for stable BTD-based fluorescent bioprobes.[14,27]

After the photophysical characterization, BTD−GTN (**1**) was further submitted to cell-imaging experiments using five different cell lines (Figures 3 and 4, and S2−S4). BTD−GTN (**1**) produced fluorescent signals at three different wavelength ranges, that is, it could be monitored at the blue, green, and red channels. This feature is very attractive toward multicolor staining procedures, which is a desirable feature for fluorescent probes, as described elsewhere.[22] This is because emission of **1**

DOI: 10.1021/acsomega.7b00416
ACS Omega 2017, 2, 3774−3784

Scheme 1. Synthesis of the BTD−GTN Hybrid (1)

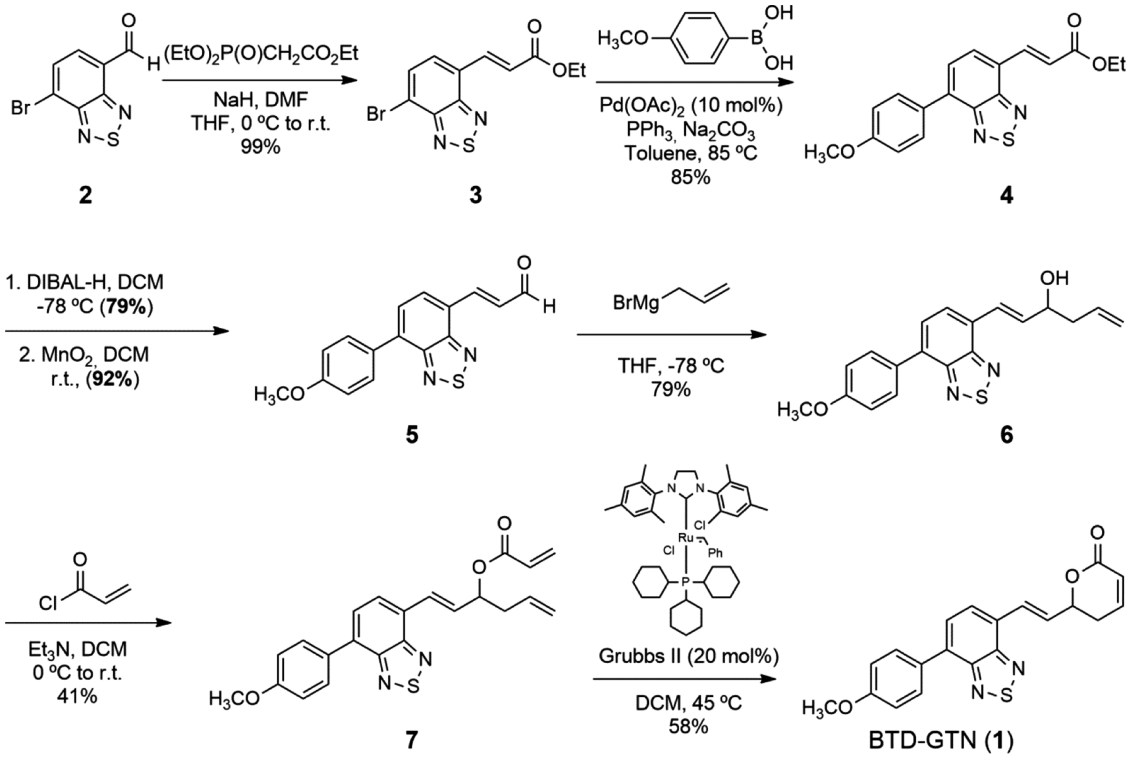

Table 1. UV−Vis and Fluorescence Emission Data (in Different Solvents) for BTD−GTN (10 μM Solutions for All Experiments)[a]

compound	solvent	λ_{max} (abs) (nm)	log ε (e)	λ_{max} (em) (nm)	Stokes shift (nm and cm^{-1})
BTD−GTN	Ph-Me	410	3.95 (8877)	514	104 (4935)
	CH_2Cl_2	405	3.98 (9527)	532	127 (5894)
	AcOEt	404	4.00 (9961)	523	119 (5632)
	CH_3CN	402	3.95 (8930)	543	141 (6459)
	dimethyl sulfoxide (DMSO)	409	3.95 (8954)	554	145 (6399)
	EtOH	405	3.94 (8730)	545	140 (6343)
	MeOH	403	3.97 (9337)	555	152 (6796)
	H_2O	417	3.91 (8233)	549	132 (5766)

[a]Quantum yield (MeCN): 0.43.

is more intense depending on the irradiation wavelength, and by selecting the appropriate photomultiplier, it is possible to acquire simultaneously the three emission colors or a specific channel, therefore facilitating the visualization of just one color with no interference of the others. No photobleaching (neither fade off) under the standard operational conditions during the image acquisition process could be noted, in accordance with the reported photostability of BTD derivatives.[15]

Confocal microscopy has shown that BTD−GTN (1) was found distributed in the cytoplasm region of Caco-2 (human colorectal cancer) cells and, to a much less extent, in the nuclei, as depicted in Figure 3. Figure 3A−D shows the live cell samples, whereas Figure 3E−H shows fixed Caco-2 cells. These results suggest that BTD−GTN (1) was slightly more accumulated in live cells than in fixed cells. All samples showed bright fluorescent signals, especially at the green wavelength, and the fluorescence intensities undergo a slight variation depending on the cell type, especially at the red channel.

These results show that BTD−GTN (1) was not preferentially found inside the nuclei of the cells under the tested experimental conditions (live or fixed cells), thus indicating a weak chemical affinity between BTD−GTN (1) and the components of the nuclei. Phase contrast images of all samples (Figure 3D,H) are shown to verify the cell morphological aspects. The same pattern was observed for MDA-MB-231 (invasive human breast adenocarcinoma), as depicted in Figure 4, and for A549 (human lung carcinoma, Figure S2), MCF-7 (breast cancer line, Figure S3), and RAW 264.7 (mouse macrophage, Figure S4) cells, as shown in the Supporting Information file.

As recently reviewed,[1] some authors have suggested that DNA damage by GTN action is followed by induced apoptosis.[28] This conclusion was later confronted by other authors, whose results indicated that GTN was responsible for the DNA-induced fragmentation.[29] In our studies, we have not observed the events above, as BTD−GTN (1) was basically accumulated in the cytosol, more specifically in the mitochondria. In fact, other reports have focused on cascade events after GTN induced mitochondrial membrane potential impairing and disbalance on the concentration of oxidizing species.[11]

DOI: 10.1021/acsomega.7b00416
ACS Omega 2017, 2, 3774−3784

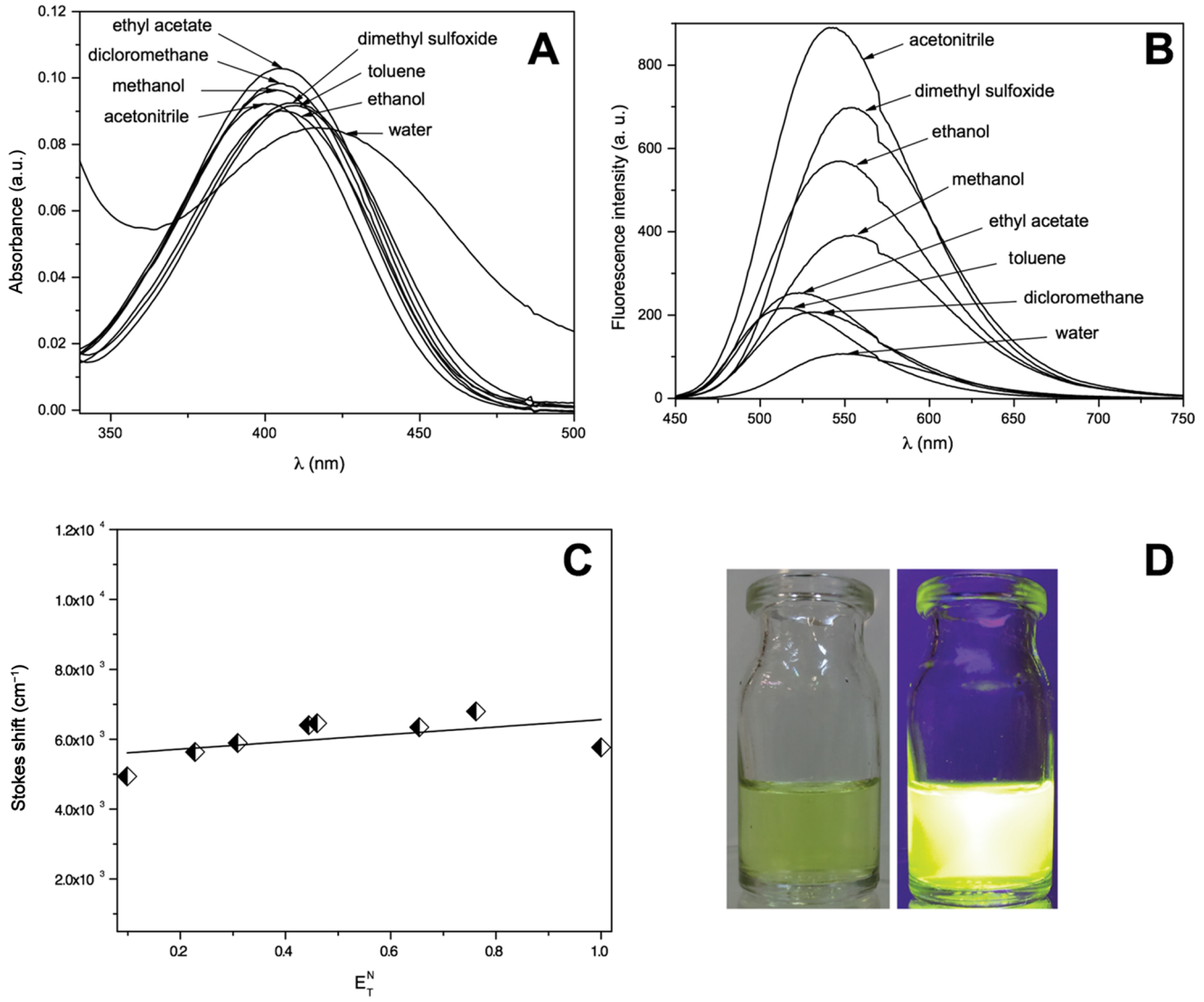

Figure 2. (A) UV−vis spectra, (B) fluorescence spectra, and (C) Stokes shift (cm^{-1}) of BTD−GTN vs E_T^N values for the tested solvents (10 mM solutions for all analyses). (D) BTD−GTN (**1**) under white light (left) and UV light irradiation (right, l_{ex} 365 nm) in acetonitrile (80 μM).

As depicted in Figure 3, BTD−GTN (**1**) was distributed in the cytoplasm and, to some extent, in the mitochondria, thus indicating the possibility of disbalance in the concentration of oxidizing species, followed by apoptosis induction through cascade events, as the role of mitochondria in cell apoptosis is well documented. Although the mechanism of the GTN action is still open to debate and the preferential accumulation site of the compound in a particular cell region does not necessarily mean this is also the preferential and single point of biological action, our results point to a mitochondrial action in line with previous literature findings. No morphological alteration could be noted using mouse macrophages (Figure S4), indicating a good level of selection of the fluorescent BTD−GTN (**1**) as that observed for natural GTN.[19,20]

To confirm the preference for mitochondrial accumulation of **1**, costaining experiments using the commercially available MitoTracker Red have been performed. As the emission intensity of BTD−GTN (**1**) at 543 nm is very weak compared to that of MitoTracker Red, we adjusted the concentrations of these two compounds so that we would be able to detect the emission by BTD−GTN (**1**) when working under the recommended concentration of Mitotracker Red, as described in Experimental Section. Figure 5A,B shows the cell cytoplasm fluorescence distribution when stained with BTD−GTN (**1**) (observed in the green channel) and MitoTracker (red emission), respectively. Figure 5C shows the fluorescence channel overlay from both compounds. The yellow arrowheads indicate the cell cytoplasm region of accumulation of **1** and MitoTracker Red. The fluorescence distribution in all samples has been therefore precisely the same for both dyes, as seen in Figure 5C, displaying a yellow emission produced by merging panels (A) and (B) in Figure 5. This result demonstrated that BTD−GTN (**1**) has indeed accumulated inside the cell mitochondria. A phase contrast image was also generated for all samples (Figure 5D) to verify the morphological aspects of the cell. It was observed that the morphological alteration in MDA-MB-231 cells, as already depicted in Figure 4, is related to the focal adhesion points, as indicated by the white arrows.

Although these morphological alterations were observed in the MDA-MB-231 cells, the mitochondria clearly could be stained by both dyes. Both compounds also showed the same cytoplasm regions of staining exclusions, as noted in Figure 6A,B, which are better observed in Figure 6C,D. These black voids found in the cell cytoplasm are likely to be endosomes

DOI: 10.1021/acsomega.7b00416
ACS Omega 2017, 2, 3774−3784

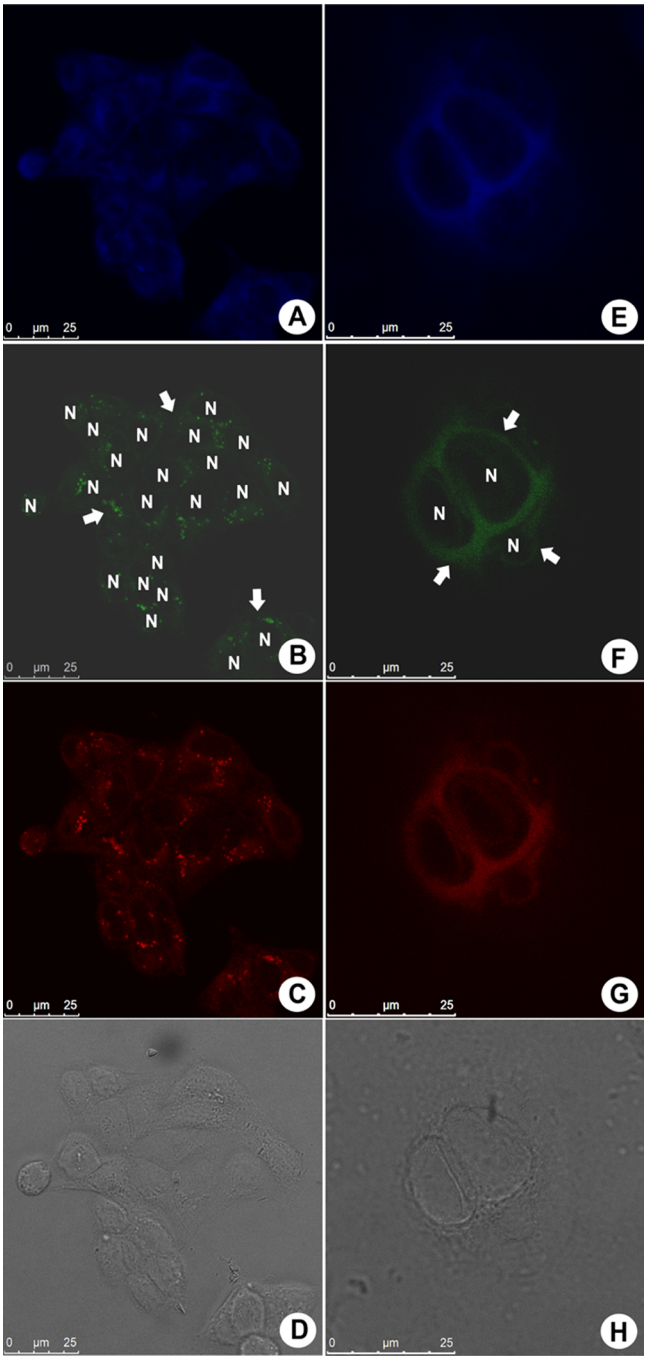

Figure 3. Fluorescence profile of Caco-2 (human epithelial colorectal adenocarcinoma) cells treated with 10 μM BTD−GTN (**1**) visualized at the blue, green, and red channels; (A)−(D) show live cells, whereas (E)−(H) show fixed cells; (D, H) morphological aspects of the samples by phase contrast microscopy. Arrows show the cytoplasm distribution of BTD−GTN (**1**), and the nuclei are shown as black voids identified by "N". The reference scale bar is 25 μm.

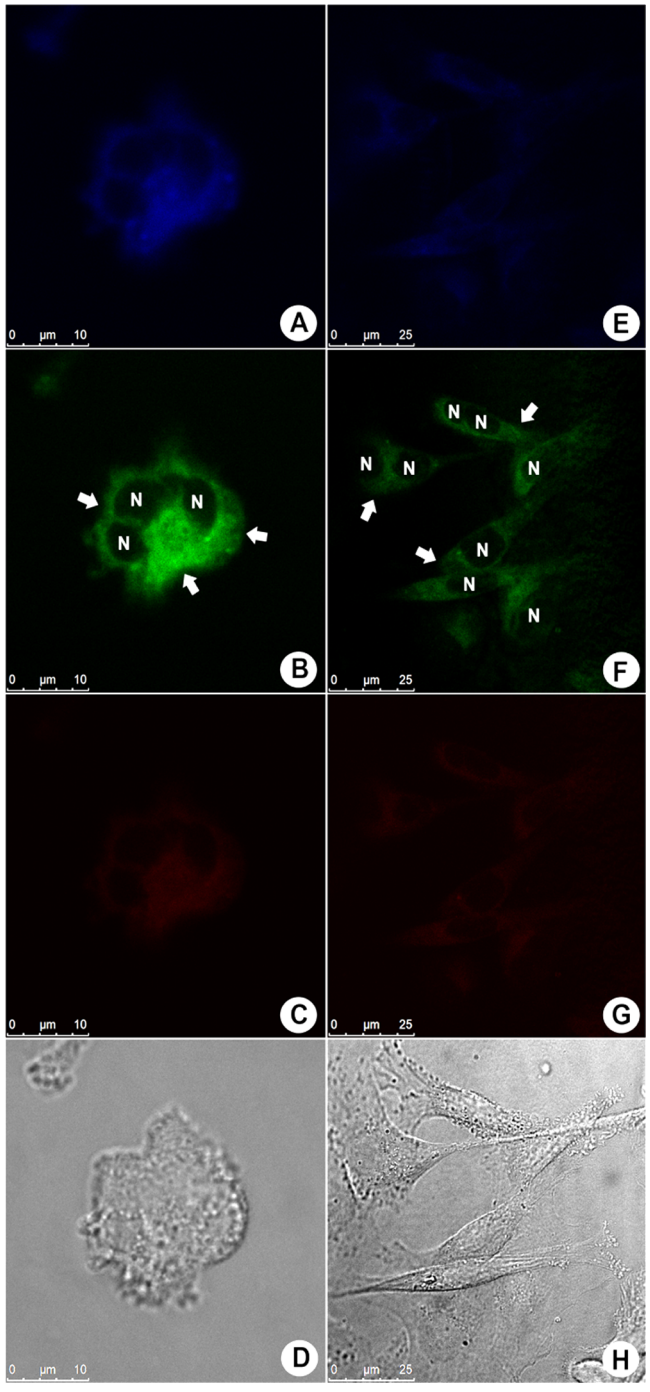

Figure 4. Fluorescence profile of MDA-MB-231 (invasive human breast adenocarcinoma) cells treated with 10 μM BTD−GTN (**1**) visualized at the blue, green, and red channels; (A)−(D) show live cells, whereas (E)−(H) show fixed cells; (D, H) morphological aspects of the samples by phase contrast microscopy. Arrows show the cytoplasm distribution of BTD−GTN (**1**), and the nuclei are shown as black voids identified by "N". The reference scale bar is 25 μm.

and lysosomes due to their relative position and apparent volumes in the cell.

To confirm these results, we performed a complementary in vitro staining assay with BTD−GTN and rhodamine 1,2,3 using MDA-MB-231 cells as a model. These assays were performed separately to avoid fluorescence crosstalk between the rhodamine 1,2,3 and BTD−GTN (**1**) emissions. The same fluorescence cellular distributions were observed for both compounds. The cells incubated with both compounds showed a mild cytoplasmic staining with a fluorescence accumulation near the cell nuclei (Figure S5). These results provide additional evidence that BTD−GTN (**1**) preferentially accumulates in mitochondria, as already observed in samples stained with the MitoTracker marker (Figure 5).

Additional in vitro experiments were performed to collect evidence for the cellular localization of GTN and BTD−GTN

DOI: 10.1021/acsomega.7b00416
ACS Omega 2017, 2, 3774−3784

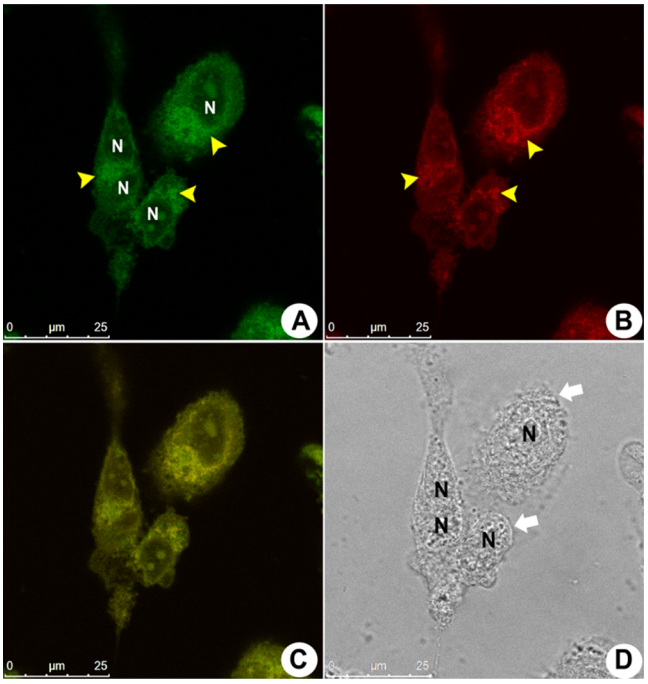

Figure 5. Fluorescence profile of MDA-MB-231 cells incubated with BTD−GTN plus MitoTracker Red. (A, B) Fluorescence patterns from cells incubated with BTD−GTN (**1**) followed in the green channel and MitoTracker Red (red emission), respectively. Yellow arrowheads indicate the same cell cytoplasm accumulation region for both compounds. (C) A nearly perfect overlay of the green and red fluorescence images from (A) and (B). (D) The morphological aspects of the samples by phase contrast microscopy. The white arrows indicate morphological alterations in the focal adhesion points of cells. The cell nuclei are shown as black voids identified by "N". The reference scale bar is 25 μm.

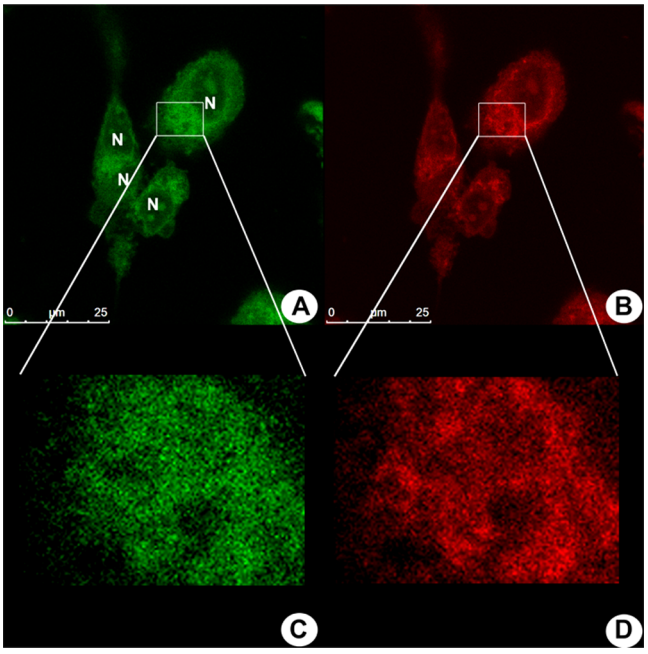

Figure 6. Same exclusion regions on the cell cytoplasm are shown in MDA-MB-231 cells incubated with BTD−GTN (**1**) and MitoTracker Red. (A, B) Cell distributions of the fluorescence signal from BTD−GTN (green) and MitoTracker Red staining, respectively. The same fluorescence exclusion regions are shown in the white rectangles. (C, D) Magnified (10-fold) images of these regions. The cell nuclei are shown as black voids identified by "N" only in the samples stained with BTD−GTN. The reference scale bar is 25 μm.

(**1**) using MDA-MB-231 cells as a model. We carried out two different assays to avoid crosstalk between BTD−GTN (**1**) and MitoTracker Red fluorescence emissions. First, the cells were preincubated with GTN, followed by treatment with Mitotracker Red. In the second experiment, the sample was prestained with MitoTracker Red and then incubated with GTN. The results of the first experiment indicated that the preincubation with GTN dislodged the MitoTracker from its mitochondrial target. As a result, the intensity of the MitoTracker emission was highly reduced (Figure 7A). When the sample was previously incubated with MitoTracker Red, no reduction in fluorescence intensity could be observed when GTN was added (Figure 7B). The quantitative analyses of fluorescence with these images show a high statistical significance related to fluorescence reduction from the sample preincubated with GTN (Figure 7E).

Next, the samples were preincubated with different concentrations of GTN and then stained with BTD−GTN (**1**). Our results showed that GTN also displaced BTD−GTN (**1**) from its mitochondrial target, lowering the fluorescence emission intensities compared to those of the samples stained only with BTD−GTN (**1**), used as a positive control (Figures S6−S9). The fluorescence intensities from the samples were calculated and analyzed. Our results showed a reduction of fluorescence intensity related to all samples against the control samples. Only the samples pretreated with a GTN solution at 2.5 μM showed fluorescence intensity reduction without statistical significance (Figure S10). In conclusion, our data strongly suggest that BTD−GTN (**1**) preferentially accumulates in the mitochondria.

As the results described above indicated the preferential localization of BTD−GTN (**1**) in the mitochondria, we considered to evaluate the effect of GTN and BTD−GTN (**1**) on the production of oxidizing species. Unfortunately, we were not able to evaluate the role of BTD−GTN (**1**) in the production of oxidizing species using the 2′,7′-dichlorodihydrofluorescein diacetate (DCFDA) assay and MDA-MB-231 cells due to the fluorescence crosstalk between DCFDA and BTD−GTN (**1**). As expected, when a 10 μM GTN solution was employed, an increase in the ROS concentration compared to that of the positive control samples was observed (Figure 8D,E). Quantification of these effects resulted in a high degree of statistical significance between the production of oxidizing species induced by GTN and the production of ROS induced by H_2O_2 (Figure 8E). An increased production of oxidizing species by mammal cells as well as other eukaryotic cell models is highly correlated with mitochondrial dysfunction and apoptosis.[30−34]

CONCLUSIONS

In summary, we have described the synthesis, characterization, and bioimaging experiments of a new BTD-containing GTN derivative. Our data show that the mechanism of action of the GTN derivative might involve a cascade of events, starting with its interaction with mitochondria, as shown here for the first time for the BTD−GTN (**1**) hybrid. Although we were not able to determine the role of BTD−GTN (**1**) in the levels of oxidizing species using MDA-MB-231 cells, the increase in their concentration in GTN-treated cells correlates well with its mitochondrial localization, as described here. These results

DOI: 10.1021/acsomega.7b00416
ACS Omega 2017, 2, 3774−3784

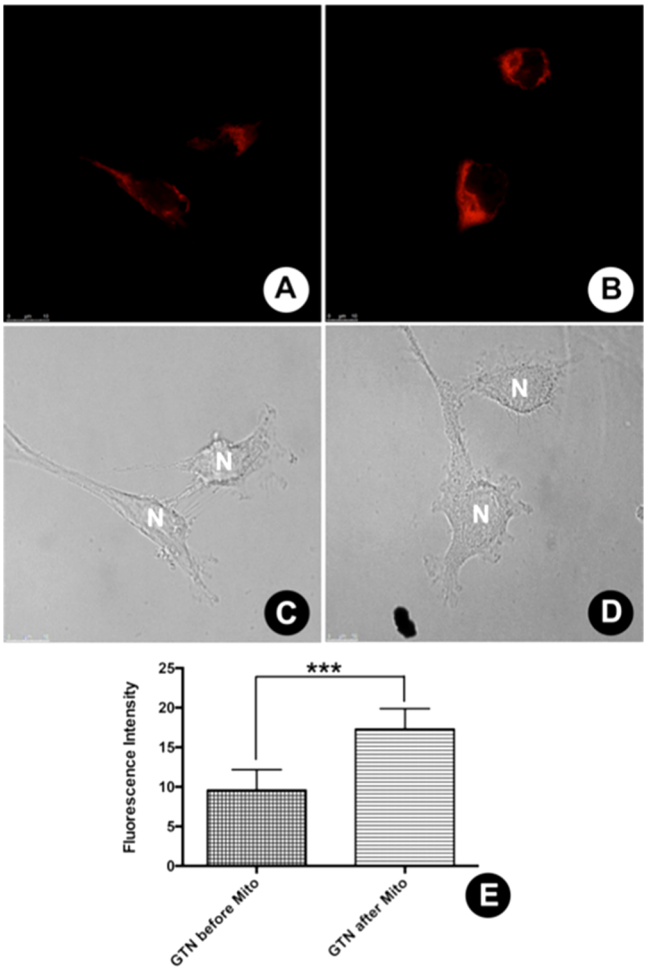

Figure 7. Fluorescence dislodge assay (GTN × MitoTracker). (A) Reduced fluorescence emission from sample preincubated with GTN, followed by incubation with MitoTracker Red. (B) Intense fluorescence emission from sample preincubated MitoTracker Red, followed by GTN incubation. (C, D) Normal morphological aspects of the cell samples by phase contrast microscopy. (E) Quantitative analyses of fluorescence intensities with a high level of statistical significance. The cell nuclei are indicated by "N". The reference scale bar is 10 μm, *** $p \leq 0.001$.

open up the possibility of exploring new fluorescent BTD-containing GTN derivatives in the investigation of the cellular mechanism of action of this important and promising class of styryl lactone derivatives. The synthesis and bioimaging experiments of new derivatives are underway and will be disclosed in due course.

EXPERIMENTAL SECTION

Chemical Synthesis. *General Information.* Starting materials and reagents were obtained from commercial sources and used as received unless otherwise specified. Dichloromethane and triethylamine were treated with calcium hydride and distilled before use. Tetrahydrofuran (THF) was treated with metallic sodium in the presence of benzophenone and distilled before use. Anhydrous dimethylformamide (DMF) was obtained from Sigma-Aldrich. Anhydrous reactions were carried out with continuous stirring under dry nitrogen atmosphere. The progress of the reactions was monitored by a thin-layer chromatography analysis (silica gel 60 F254 on aluminum plates; Merck). Purification by flash chromatography was performed using silica gel 60, 0.035−0.070 mm (Merck). Melting points were determined on Electrothermal 9100 model equipment and were not corrected. ^{1}H NMR spectra were recorded at 250 or 500 MHz, ^{13}C NMR spectra were recorded at 62.5 or 125 MHz, and the chemical shifts were reported in parts per million (ppm) relative to the deuterated solvent as the internal standard ($CDCl_3$ 7.26 ppm, 77.0 ppm) and coupling constants (J) in hertz (Hz). Mass spectra were recorded on a Waters Xevo QTof apparatus operating in the electrospray mode. IUPAC names of the compounds were generated using ChemBioDraw Ultra 12.0. The NMR spectra were processed using ACD/NMR Processor Academic Edition version 12.0.

*(E)-Ethyl-3-(7-bromobenzo[c][1,2,5]thiadiazol-4-yl)-acrylate (**3**).* To a suspension of NaH (107 mg, 2.67 mmol) and triethyl phosphonoacetate (0.47 mL, 2.3 mmol) in dry DMF (0.6 mL) and dry THF (4 mL) at 0 °C under nitrogen atmosphere, a solution of 7-bromobenzo[c][1,2,5]thiadiazole-4-carbaldehyde (**2**) (446 mg, 1.78 mmol) in dry THF (24 mL) was added. The reaction mixture was allowed to warm to room temperature (rt), and after 60 min, the solvent was removed under reduced pressure and the residue was purified by flash chromatography (SiO_2, Hex/AcOEt 70:30).

Yellow solid. Yield: 557 mg, 1.78 mmol, 99%; mp 135−137 °C.

^{1}H NMR (250 MHz, $CDCl_3$) δ ppm 1.35 (t, J = 7.1 Hz, 3H, CH_3), 4.29 (q, J = 7.1 Hz, 2H, CH_2), 7.41 (d, J = 16.1 Hz, 1H, CH), 7.53 (d, J = 7.6 Hz, 1H, CH), 7.79−7.95 (m, 2H, 2 × CH).

^{13}C NMR (62.5 MHz, $CDCl_3$) δ ppm 14.3 (CH_3), 60.8 (CH_2), 116.2 (C), 124.2 (CH), 127.3 (C), 131.5 (CH), 132.0 (CH), 139.0 (CH), 152.5 (C), 153.8(C), 166.9 (CO).

HRMS (ESI+) m/z: calcd for $C_{11}H_{10}BrN_2O_2S$ [M + H$^+$], 314.9626; found, 314.9585.

*(E)-Ethyl-3-(7-(4-methoxyphenyl)benzo[c][1,2,5]-thiadiazol-4-yl)acrylate (**4**).* In a Schlenk flask kept under nitrogen atmosphere, bromide **3** (398 mg, 1.27 mmol), 4-methoxyphenyl boronic acid (244 mg, 1.52 mmol), palladium-(II) acetate (29 mg, 0.13 mmol), triphenylphosphine (185 mg, 0.699 mmol), sodium carbonate aqueous solution (2 mol L^{-1}, 1.3 mL, 2.5 mmol), and dry toluene (13 mL) were added successively. The reaction was refluxed at 85 °C for 24 h. The reaction mixture was directly purified by flash chromatography (SiO_2, Hex/AcOEt 80:20).

Yellow solid. Yield: 368 mg, 1.08 mmol, 85%; mp 124−126 °C.

^{1}H NMR (250 MHz, $CDCl_3$) δ ppm 1.38 (t, J = 7.1 Hz, 3H, CH_3), 3.89 (s, 3H, OCH_3), 4.32 (q, J = 7.1 Hz, 2H, CH_2), 7.06 (d, J = 9.0 Hz, 2H, 2 × CH), 7.49 (d, J = 16.0 Hz, 1H, CH), 7.66 (d, J = 7.4 Hz, 1H, CH), 7.75 (d, J = 7.4 Hz, 1H, CH), 7.92 (d, J = 9.0 Hz, 2H, 2 × CH), 8.03 (d, J = 16.0 Hz, 1H, CH).

^{13}C NMR (62.5 MHz, $CDCl_3$) δ ppm 14.3 (CH_3), 55.4 (CH_3), 60.6 (CH_2), 114.1 (CH), 122.8 (CH), 126.0 (C), 126.7 (CH), 129.3 (C), 130.6 (CH), 131.9 (CH), 135.5(C), 140.0 (CH), 153.7 (C), 154.0 (C), 160.2 (C), 167.4 (CO).

HRMS (ESI+) m/z: calcd for $C_{18}H_{17}N_2O_3S$ [M + H$^+$], 341.0960; found, 341.1009.

(E)-3-(7-(4-Methoxyphenyl)benzo[c][1,2,5]thiadiazol-4-yl)-prop-2-en-1-ol. To a solution of ester **4** (360 mg, 1.06 mmol) in dry dichloromethane (22 mL) at −78 °C and under nitrogen atmosphere, a solution of diisobutylaluminum hydride (0.47 mL, 2.6 mmol) in dry dichloromethane (5 mL) was added. The reaction mixture was stirred for 30 min and warmed to 0 °C.

DOI: 10.1021/acsomega.7b00416
ACS Omega 2017, 2, 3774−3784

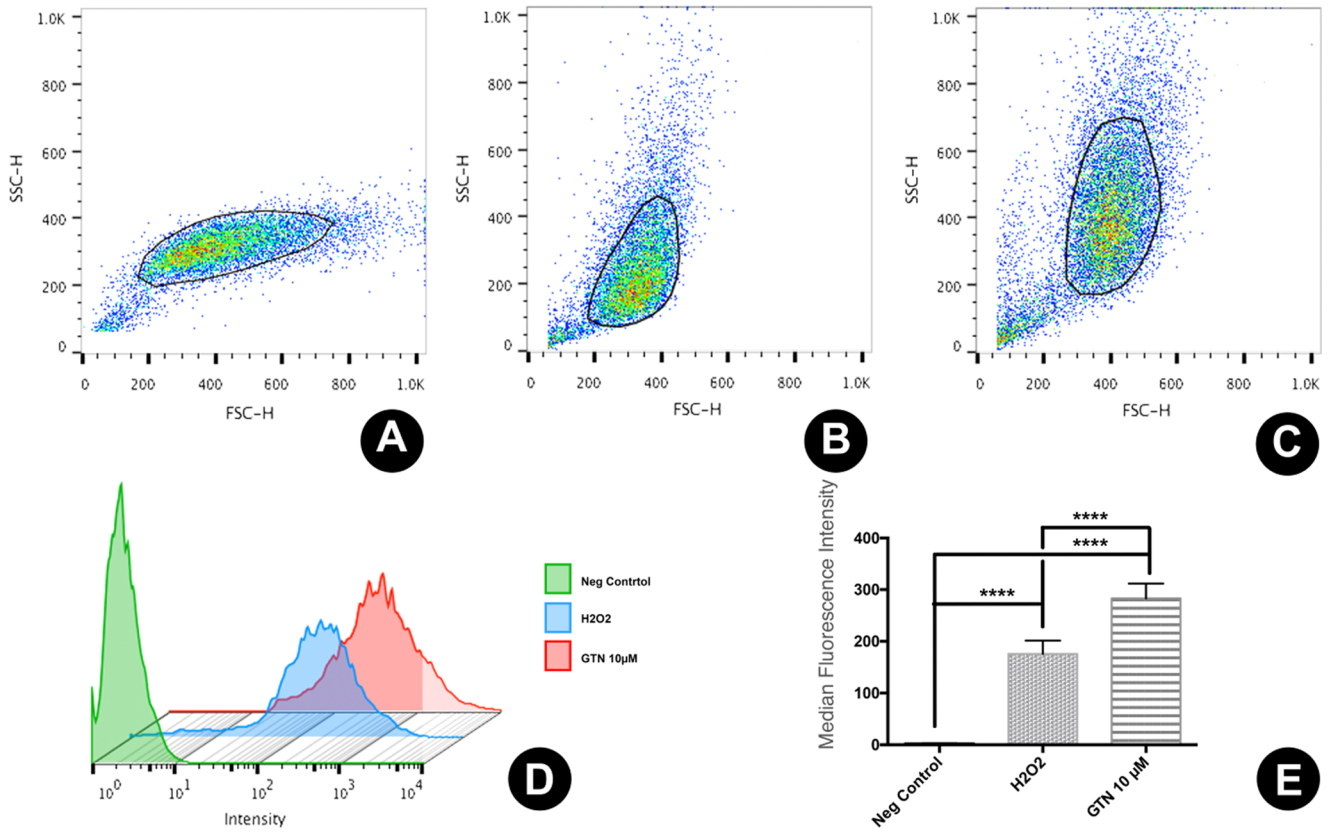

Figure 8. Flow cytometry for ROS detection. (A–C) Sample morphologies under different assay conditions: negative control, H_2O_2 stimulation, and GTN incubation, respectively. The boundary area is the acquisition gate. (D) Histogram of fluorescence intensity related to the production of oxidizing species under all experimental conditions. (E) Quantitative analyses with a high level of statistical significance from the median of fluorescence intensities obtained. **** $p \leq 0.0001$.

Then, ethyl acetate (1.6 mL) was added slowly, followed by a slow addition of 1 M HCl (9.2 mL). The mixture was stirred for 14 h at rt and extracted with dichloromethane (3 × 15 mL). The combined organic phases were dried over $MgSO_4$. The solvent was removed under reduced pressure, and the residue was purified by flash chromatography (SiO_2, Hex/AcOEt 60:40).

Yellow solid. Yield: 250 mg, 0.838 mmol, 79%; mp 122–123 °C.

^{1}H NMR (250 MHz, $CDCl_3$) δ ppm 3.89 (s, 3H, OCH_3), 4.48 (d, J = 4.6 Hz, 2H, CH_2), 7.06 (d, J = 8.9 Hz, 2H, 2 × CH), 7.14–7.34 (m, 2H, 2 × CH), 7.61 (s, 2H, 2 × CH), 7.89 (d, J = 8.9 Hz, 2H, 2 × CH).

^{13}C NMR (62.5 MHz, $CDCl_3$) δ ppm 55.4 (CH_3), 63.9 (CH_2), 114.1 (CH), 126.5 (CH), 127.1 (CH), 127.3 (CH), 128.2 (C), 129.8 (C), 130.4 (CH), 132.8 (C), 133.6 (CH), 153.9 (C), 154.0 (C), 159.8 (C).

HRMS (ESI+) m/z: calcd for $C_{16}H_{13}N_2OS$ [$(M+H^+) - H_2O$], 281.0749; found, 281.0722.

*(E)-3-(7-(4-Methoxyphenyl)benzo[c][1,2,5]thiadiazol-4-yl)-acrylaldehyde (**5**).* A suspension of the above-described alcohol (222 mg, 0.745 mmol) and activated manganese dioxide (720 mg, 7.45 mmol) in dichloromethane (12 mL) was stirred for 1 h. The reaction mixture was filtered through a pad of Celite. The solvent was removed under reduced pressure to obtain aldehyde **4**, which was used in the next step without purification.

Yellow solid. Yield: 204 mg, 0.688 mmol, 92%; mp 187–188 °C.

^{1}H NMR (250 MHz, $CDCl_3$) δ ppm 3.90 (s, 3H, OCH_3), 7.09 (d, J = 9.0 Hz, 2H, 2 × CH), 7.61 (dd, J = 16.0, 7.7 Hz, 1H, CH), 7.73 (d, J = 7.4 Hz, 1H, CH), 7.81–8.07 (m, 4H, 4 × CH), 9.84 (d, J = 7.7 Hz, 1H, CHO).

^{13}C NMR (62.5 MHz, $CDCl_3$) δ ppm 55.4 (CH_3), 114.3 (CH), 125.6 (C), 126.6 (CH), 129.1 (C), 130.7 (CH), 131.6 (CH), 132.0 (CH), 136.6 (C), 147.4 (CH), 153.7 (C), 153.9 (C), 160.5 (C), 194.2 (CHO).

HRMS (ESI+) m/z: calcd for $C_{16}H_{13}N_2O_2S$ [$M + H^+$], 297.0698; found, 297.0668.

*(E)-1-(7-(4-Methoxyphenyl)benzo[c][1,2,5]thiadiazol-4-yl)-hexa-1,5-dien-3-ol (**6**).* To a solution of aldehyde **5** (203 mg, 0.686 mmol) in dry THF (45 mL) under nitrogen atmosphere at −78 °C, a commercial 1 M solution of allylmagnesium bromide in diethyl ether (2.1 mL, 2.1 mmol) was added. The reaction mixture was stirred for 30 min under these conditions and let to reach rt. Saturated aqueous ammonium chloride (2.7 mL) was added, and the layers were separated. The aqueous layer was extracted with diethyl ether (3 × 10 mL). The combined organic phases were dried over $MgSO_4$. The solvent was removed under reduced pressure, and the residue was purified by flash chromatography (SiO_2, Hex/AcOEt 70:30).

Yellow solid. Yield: 183 mg, 0.541 mmol, 79%; mp 76–77 °C.

^{1}H NMR (250 MHz, $CDCl_3$) δ ppm 1.96 (br s, 1H, OH), 2.38–2.66 (m, 2H, CH_2), 3.89 (s, 3H, OCH_3), 4.41–4.62 (m, 1H, CH), 5.11–5.35 (m, 2H, CH_2), 5.80–6.04 (m, 1H, CH), 7.06 (d, J = 8.9 Hz, 2H, 2 × CH), 7.11–7.20 (m, 2H, 2 × CH), 7.61 (s, 2H, 2 × CH), 7.90 (d, J = 8.9 Hz, 2H, 2 × CH).

DOI: 10.1021/acsomega.7b00416
ACS Omega 2017, 2, 3774–3784

^{13}C NMR (62.5 MHz, $CDCl_3$) δ ppm 42.1 (CH_2), 55.4 (CH_2), 71.9 (CH), 114.1 (CH), 118.7 (CH_2), 126.0 (CH), 127.1 (CH), 127.4 (CH), 128.2 (C), 129.9 (C), 130.4 (CH), 132.8 (C), 134.0 (CH), 136.6 (CH), 153.9 (C), 154.0 (C), 159.8 (C).

HRMS (ESI+) m/z: calcd for $C_{19}H_{17}N_2OS$ [$(M+H^+) - H_2O$], 321.1062; found, 321.1035.

(E)-1-(7-(4-Methoxyphenyl)benzo[c][1,2,5]thiadiazol-4-yl)-hexa-1,5-dien-3-yl acrylate (7). To a solution of homoallylic alcohol **6** (162 mg, 0.478 mmol) in dry dichloromethane (10 mL) under inert atmosphere and at rt, triethylamine (135 μL, 0.956 mmol) was added. The reaction mixture was stirred for 30 min at rt when it was cooled to 0 °C, and acryloyl chloride (61 μL, 0.72 mmol) was added dropwise. The mixture reaction mixture was warmed to rt and then stirred for 30 min when the solvent was removed under reduced pressure, and the crude product obtained was purified by flash chromatography (SiO_2, Hex/AcOEt 70:30).

Yellow liquid. Yield: 77 mg, 0.20 mmol, 41%.

^{1}H NMR (250 MHz, $CDCl_3$) δ ppm 2.64 (t, J = 6.7 Hz, 2H, CH_2), 3.89 (s, 3H, OCH_3), 5.07−5.24 (m, 2 H, CH_2), 5.69 (q, J = 6.3 Hz, 1H, CH), 5.77−5.99 (m, 2H, CH_2), 6.11−6.28 (m, 1H, CH), 6.38−6.60 (m, 1H, CH), 7.00−7.20 (m, 4 H, 4 × CH), 7.61 (d, J = 1.0 Hz, 2H, 2 × CH), 7.90 (d, J = 8.9 Hz, 2H, 2 × CH).

^{13}C NMR (62.5 MHz, $CDCl_3$) δ ppm 39.2 (CH_2), 55.4 (CH_3), 74.3 (CH), 114.1 (CH), 118.3 (CH_2), 127.0 (CH), 127.7 (C), 128.2 (CH), 128.4 (CH), 128.7 (CH_2), 129.8 (C), 130.4 (CH), 130.9 (CH), 132.1 (CH), 133.0 (CH), 133.2 (C), 153.8 (C), 154.1 (C), 159.9 (C), 165.5 (CO).

HRMS (ESI+) m/z: calcd for $C_{22}H_{21}N_2O_3S$ [M + H^+], 393.1273; found, 393.1287.

(E)-6-(2-(7-(4-Methoxyphenyl)benzo[c][1,2,5]thiadiazol-4-yl)vinyl)-5,6-dihydro-2H-pyran-2-one (1). To a solution of acrylate 7 (64 mg, 0.16 mmol) in dichloromethane (13 mL) under reflux, Grubbs' second-generation catalyst (14 mg, 0.016 mmol) in dichloromethane (3 mL) was added. The reaction mixture was stirred for 30 min when more Grubbs' second-generation catalyst (14 mg, 0.016 mmol) dissolved in dichloromethane (3 mL) was added. After 4.5 h, the reaction mixture was cooled to rt and dimethyl sulfoxide (0.12 mL, 1.6 mmol) was added. The mixture was stirred for 5 h, and the solvent was removed under reduced pressure. The crude product was purified by flash chromatography (SiO_2, Hex/AcOEt 60:40), and compound **1** was recrystallized from hexane/ethyl acetate.

Yellow solid. Yield: 35 mg, 0.095 mmol, 58%; mp 145−146 °C.

^{1}H NMR (500 MHz, $CDCl_3$) δ ppm 2.58−2.71 (m, 2H, CH_2), 3.89 (s, 3H, OCH_3), 5.21−5.29 (m, 1H, CH), 6.13 (dt, J = 9.8, 1.7 Hz, 1H, CH), 6.97 (ddd, J = 9.8, 5.1, 3.3 Hz, 1H, CH), 7.07 (d, J = 8.9 Hz, 2H, 2 × CH), 7.16−7.23 (m, 1H, CH), 7.28−7.34 (m, 1H, CH), 7.60−7.66 (m, 2H, 2 × CH), 7.90 (d, J = 8.9 Hz, 2H, 2 × CH).

^{13}C NMR (125 MHz, $CDCl_3$) δ ppm 29.9 (CH_2), 55.4 (CH_3), 78.0 (CH), 114.1 (CH), 121.7 (CH), 127.0 (CH), 127.2 (C), 128.8 (CH), 128.8 (CH), 129.6 (C), 130.4 (CH), 130.6 (CH), 133.6 (C), 144.7 (CH), 153.6 (C), 154.1 (C), 159.9 (C), 163.9 (CO).

HRMS (ESI+) m/z: calcd for $C_{20}H_{17}N_2O_3S$ [M + H^+], 365.0960; found, 365.1026.

Biological Studies. *Cell Culture.* MCF-7 (human breast adenocarcinoma cell), MDA-MB-231 (human breast invasive adenocarcinoma cell), Caco-2 (human epithelial colorectal adenocarcinoma cells), A549 (human lung adenocarcinoma alveolar cells), and RAW 264.7 (mouse leukemic monocyte macrophage) cells were maintained in an appropriate culture medium, as recommended by American Type Culture Collection, supplemented with 10% of fetal bovine serum plus 100 IU mL^{-1} penicillin and 100 μg mL^{-1} streptomycin at 37 °C, in a 5% CO_2 atmosphere.

BTD−GTN (1) Fluorescence Assays. Cells were seeded on 13 mm round glass coverslips on the bottom of a 24-well plate, allowed to adhere overnight, and washed three times with a serum-free medium to remove nonadherent cells. After reaching confluence, the cells were separated in two samples (live samples and fixed samples). Live cells were incubated for 30 min with a 10 μM of BTD−GTN (**1**) solution at 37 °C. The samples were washed three times with phosphate-buffered saline (PBS) 1× (pH 7.4) at rt and fixed with formaldehyde (3.7%) for 30 min. The samples were washed again three times with PBS 1× (pH 7.4) at rt, and the coverslips were mounted over the glass slides using ProLong Gold Antifade (Invitrogen, OR) according to manufacturer's recommendations. The fixed samples were first washed three times in PBS 1× (pH 7.4) and then fixed with formaldehyde (3.7%) for 30 min. After fixative procedures, the samples were washed three times in PBS 1× (pH 7.4) at rt and incubated for 30 min with a 10 μM of BTD−GTN solution at rt. The samples were washed three times in PBS 1× (pH 7.4) at rt, and the coverslips were mounted over the glass slides using ProLong Gold Antifade (Invitrogen, OR) according to manufacturer's recommendations. The negative control was performed by incubating the cells in 0.1% of DMSO, which was the diluent used. The samples were analyzed using a Leica TCS SP5 confocal microscope. The wavelength used to promote the BTD−GTN (**1**) excitation was 405 nm. The monitoring emission windows were 440−480 nm (blue), 520−560 nm (green), and 680−720 nm (red). All assays were performed in triplicate and in three repetitions for each cell sample and experimental condition.

Costaining with MitoTracker. To confirm the morphological evidence that BTD−GTN (**1**) was accumulated in mitochondria, the compound was used in a costaining assay with the commercial mitochondria marker MitoTracker Red (Thermo Fisher Scientific Inc., NY). Briefly, 3 × 10^5 cells were seeded on 13 mm round glass coverslips on the bottom of a 24-well plate, allowed to adhere overnight, and washed three times with a serum-free medium to remove nonadherent cells. After reaching confluence, the samples were incubated for 30 min at 37 °C with 10 μM of BTD−GTN (**1**) plus 100 nM of MitoTracker Red. The samples were washed three times in PBS (pH 7.4) at 37 °C, and the cells were fixed in a 3.7% formaldehyde solution for 30 min at rt. The samples were washed three times in PBS, and the coverslips were mounted over the glass slides using ProLong Gold Antifade (Invitrogen, OR) according to manufacturer's recommendations. The negative control was performed by incubation of the samples in solutions down to 0.1% of DMSO, which was used as the BTD−GTN (**1**) diluent. The samples were analyzed using a Leica TCS SP5 confocal microscope, according to manufacturer's specifications of MitoTracker Red. All assays were performed in triplicate and in three independent repetitions.

BTD−GTN (1) and Rhodamine 1,2,3 Fluorescence Assays. MDA-MB-231 cells (3 × 10^5 cells) were seeded on 13 mm glass coverslips placed at the bottom of a 24-well plate and allowed to adhere overnight. After reaching confluence, the cell

DOI: 10.1021/acsomega.7b00416
ACS Omega 2017, 2, 3774−3784

samples were treated with 10 μM BTD−GTN (**1**) and rhodamine 1,2,3 (10 μg mL^{-1}) for 30 min at 37 °C. The cells were washed three times with PBS 1× (pH 7.4) and submitted to the fixation procedure with 3.7% formaldehyde for 15 min. The samples were washed three times with PBS and mounted over glass slides with ProLong Gold Antifade (Invitrogen, OR). The samples were analyzed using a Leica TCS SP5 confocal microscope. Both BTD−GTN (**1**) and rhodamine 1,2,3 were excited with a laser wavelength of 405 nm. All assays were performed in triplicate, and three repetitions were carried out for each experimental condition.

Fluorescence Dislodge Assay (GTN × MitoTracker). MDA-MB-231 cells (3 × 10^5 cells) were seeded on 13 mm glass coverslips placed at the bottom of a 24-well plate and allowed to adhere overnight. After reaching confluence, the cells were split into four different samples. Each sample was incubated following two different protocols: (1) the samples were previously incubated with a GTN solution (10 μM) for 30 min at 37 °C, washed three times in PBS 1×, and then incubated with MitoTracker (500 nM) for 30 min; (2) the remaining samples were previously incubated with MitoTracker (500 nM) for 30 min, washed three times in PBS 1×, and then incubated with a 10 μM GTN solution for 30 min. After the staining procedures, all samples were washed again three times with PBS 1× and submitted to the fixation procedure with 3.7% formaldehyde for 15 min. The samples were washed three times in PBS and mounted over glass slides with ProLong Gold Antifade (Invitrogen, OR). The samples were analyzed using a Leica TCS SP5 confocal microscope. MitoTracker was excited with a 543 nm laser wavelength. All assays were performed in triplicate, and three repetitions were carried out for each experimental condition.

Fluorescence Dislodge Assay (GTN × BTD−GTN). MDA-MB-231 cells (3 × 10^5 cells) were seeded on 13 mm glass coverslips placed at the bottom of a 24-well plate and allowed to adhere overnight. After reaching confluence, the cells were submitted to the fixation procedure with 3.7% formaldehyde for 15 min. The samples were washed three times in PBS 1× and split into four different samples. Each sample was incubated with a GTN solution at specific concentrations (2.5, 5.0, 7.5, and 10 μM) for 30 min at 37 °C. The samples were washed three times with PBS 1× (pH 7.4) and incubated with BTD−GTN for 30 min, followed by washing three times with PBS 1×. The positive control was performed by samples incubated only with BTD−GTN (**1**) at 10 μM, under the same conditions described above. All samples were mounted over glass slides with ProLong Gold Antifade (Invitrogen, OR). The samples were analyzed using a Leica TCS SP5 confocal microscope. BTD−GTN (**1**) was excited with a 405 nm laser wavelength. All assays were performed in triplicate, and three repetitions were carried out for each experimental condition.

Flow Cytometry for the Detection of Oxidizing Species. The generation of oxidizing species was measured by staining MDA-MB-231 cells with DCFDA (Sigma-Aldrich, St. Louis, MO). MDA-MB-231 cells (1 × 10^5 cells per well) were seeded on a 24-well plate, allowed to adhere overnight, and washed three times with PBS 1× (pH 7.4) to remove nonadherent cells. After reaching confluence, the cells were submitted to the following staining procedures: the samples were preincubated with 25 μM DCFDA (35845; Sigma-Aldrich) for 45 min at 37 °C, washed three times with PBS 1× (pH 7.4), and treated with a 10 μM GTN solution for 30 min at 37 °C. Hydrogen peroxide (100 mM for 20 min) was used as a positive control to validate the protocol. After staining, the cells were washed with PBS 1× (pH 7.4) at rt and submitted to a trypsinization procedure at 37 °C for the removal of the cells from the plate. The cells were analyzed in a FACSCalibur (BD Biosciences) cytometer through 1 × 10^4 events in the gate. All assays were performed in triplicate, and five repetitions were carried out for each experimental condition.

Quantitative Analyses. The quantitative analyses of fluorescence emission intensity were performed using 10 different images in ImageJ free software.[35] The flow cytometry data were analyzed using FlowJo software version 10.0 (TriStar Inc., CA). All numerical data were submitted to statistical analysis through Prism GraphPad Software version 5.00 for MacOS (GraphPad Software; La Jolla, CA).

■ ASSOCIATED CONTENT

Supporting Information

The Supporting Information is available free of charge on the ACS Publications website at DOI: 10.1021/acsomega.7b00416.

Photostability graphs; fluorescence profiles; costaining profile; fluorescence dislodge assays; quantitative analyses of fluorescence emission intensities from fluorescence dislodge assay; ^{1}H and ^{13}C NMR spectra (PDF)

■ AUTHOR INFORMATION

Corresponding Authors

*E-mail: correa@unb.br (J.R.C.).
*E-mail: brenno.ipi@gmail.com (B.A.D.N.).
*E-mail: pilli@iqm.unicamp.br (R.A.P.).

ORCID

Ronaldo A. Pilli: 0000-0002-5919-7763

Notes

The authors declare no competing financial interest.

■ ACKNOWLEDGMENTS

The authors acknowledge financial support from Fundação de Amparo a Pesquisa do Estado de São Paulo (Grant nos. 2009/51602-5, 2013/07607-8, and 2016/12541-4), Conselho Nacional de Desenvolvimento Científico e Tecnológico (Grant nos. 302236/2009-0 and 140484/2012-4), CAPES (0239/16-0 and 004/2014 (CAPES/Drug Discovery Program), and FAEPEX (Grant no. 2400/16).

■ REFERENCES

(1) Seyed, M. A.; Jantan, I.; Bukhari, S. N. A. Emerging Anticancer Potentials of Goniothalamin and its Molecular Mechanisms. *BioMed Res. Int.* **2014**, *2014*, No. 536508, DOI: 10.1155/2014/536508.

(2) de Fátima, Â.; Kohn, L. K.; de Carvalho, J. E.; Pilli, R. A. Cytotoxic Activity of (*S*)-Goniothalamin and Analogues against Human Cancer Cells. *Bioorg. Med. Chem.* **2006**, *14*, 622−631.

(3) Barcelos, R. C.; Pastre, J. C.; Caixeta, V.; Vendramini-Costa, D. B.; de Carvalho, J. E.; Pilli, R. A. Synthesis of Methoxylated Goniothalamin, Aza-Goniothalamin and γ-Pyrones and their in Vitro Evaluation against Human Cancer Cells. *Bioorg. Med. Chem.* **2012**, *20*, 3635−3651.

(4) Vendramini-Costa, D. B.; de Castro, I. B. D.; Ruiz, A. L. T. G.; Marquissolo, C.; Pilli, R. A.; de Carvalho, J. E. Effect of Goniothalamin on the Development of Ehrlich Solid Tumor in Mice. *Bioorg. Med. Chem.* **2010**, *18*, 6742−6747.

(5) Vendramini-Costa, D. B.; Monteiro, K. M.; Iwamoto, L. H.; Jorge, M. P.; Tinti, S. V.; Pilli, R. A.; de Carvalho, J. E. Gastroprotective Effects of Goniothalamin against Ethanol and Indomethacin-Induced Gastric Lesions in Rats: Role of Prostaglandins,

Nitric Oxide and Sulfhydryl Compounds. *Chem. Biol. Interact.* **2014**, *224*, 206−212.
(6) Vendramini-Costa, D. B.; Spindola, H. M.; de Mello, G. C.; Antunes, E.; R. A. Pilli, R. A.; de Carvalho, J. E. Anti-Inflammatory and Antinociceptive Effects of Racemic Goniothalamin, a Styryl Lactone. *Life Sci.* **2015**, *139*, 83−90.
(7) Kido, L. A.; Montico, F.; Sauce, R.; Macedo, A. B.; Minatel, E.; Vendramini Costa, D. B.; de Carvalho, J. E.; Pilli, R. A.; Cagnon, V. H. A. Anti-Inflammatory Therapies in TRAMP Mice: Delay in PCa Progression. *Endocr.-Relat. Cancer* **2016**, *23*, 235−250.
(8) Vendramini-Costa, D. B.; Alcaide, A.; Pelizzaro-Rocha, K. J.; Talero, E.; Ávila-Román, J.; Garcia-Mauriño, S.; Pilli, R. A.; de Carvalho, J. E.; Motilva, V. Goniothalamin Prevents the Development of Chemically Induced and Spontaneous Colitis in Rodents and Induces Apoptosis in the HT-29 Human Colon Tumor Cell Line. *Toxicol. Appl. Pharmacol.* **2016**, *300*, 1−12.
(9) Chen, W.-Y.; Wu, C.-C.; Lan, Y.-H.; Chang, F.-R.; Teng, C.-M.; Wu, Y.-C. Goniothalamin induces cell cycle-specific apoptosis by modulating the redox status in MDA-MB-231 cells. *Eur. J. Pharmacol.* **2005**, *522*, 20−29.
(10) Inayat-Hussain, S. H.; Annuar, B. O.; Din, L. B.; Ali, A. M.; Ross, D. Loss Of Mitochondrial Transmembrane Potential and Caspase-9 Activation During Apoptosis Induced by the Novel Styryl-Lactone Goniothalamin in HL-60 Leukemia Cells. *Toxicol. In Vitro* **2003**, *17*, 433−439.
(11) de Fátima, Â.; Zambuzzi, W. F.; Modolo, L. V.; Tarsitano, C. A. B.; Gadelha, F. R.; Hyslop, S.; de Carvalho, J. E.; Salgado, I.; Ferreira, C. V.; Pilli, R. A. Cytotoxicity of Goniothalamin Enantiomers in Renal Cancer Cells: Involvement of Nitric Oxide, Apoptosis and Autophagy. *Chem. Biol. Interact.* **2008**, *176*, 143−150.
(12) Neto, B. A. D.; Lapis, A. A. M.; da Silva, E. N., Jr.; Dupont, J. 2,1,3-Benzothiadiazole and Derivatives: Synthesis, Properties, Reactions, and Applications in Light Technology of Small Molecules. *Eur. J. Org. Chem.* **2013**, *2013*, 228−255.
(13) Neto, B. A. D.; Correa, J. R.; Silva, R. G. Selective Mitochondrial Staining with Small Fluorescent Probes: Importance, Design, Synthesis, Challenges and Trends for New Markers. *RSC Adv.* **2013**, *3*, 5291−5301.
(14) Neto, B. A. D.; Carvalho, P. H. P. R.; Correa, J. R. Benzothiadiazole Derivatives as Fluorescence Imaging Probes: Beyond Classical Scaffolds. *Acc. Chem. Res.* **2015**, *48*, 1560−1569.
(15) Yao, S.; Kim, B.; Yue, X.; Gomez, M. Y. C.; Bondar, M. V.; Belfield, K. V. Synthesis of Near-Infrared Fluorescent Two-Photon-Absorbing Fluorenyl Benzothiadiazole and Benzoselenadiazole Derivatives. *ACS Omega* **2016**, *1*, 1149−1156.
(16) Chen, C.; Hua, Y.; Hu, Y.; Fang, Y.; Ji, S.; Yang, Z.; Ou, C.; Kong, D.; Ding, D. Far-red/near-infrared fluorescence light-up probes for specific in vitro and in vivo imaging of a tumour-related protein. *Sci. Rep.* **2016**, *6*, No. 23190.
(17) Liou, S.-Y.; Ke, C.-S.; Chen, J.-H.; Luo, Y.-W.; Kuo, S.-Y.; Che, Y.-H.; Fang, C.-C.; Wu, C.-Y.; Chiang, C.-M.; Chan, Y.-H. Tuning the Emission of Semiconducting Polymer Dots from Green to Near-Infrared by Alternating Donor Monomers and Their Applications for in Vivo Biological Imaging. *ACS Macro Lett.* **2016**, *5*, 154−157.
(18) Abate, C.; Hornick, J. R.; Spitzer, D.; Hawkins, W. G.; Niso, M.; Perrone, R.; Berardi, F. Fluorescent Derivatives of σ Receptor Ligand 1-Cyclohexyl-4-[3-(5-methoxy-1,2,3,4-tetrahydronaphthalen-1-yl)-propyl]piperazine(PB28) as a Tool for Uptake and Cellular Localization Studies in Pancreatic Tumor Cells. *J. Med. Chem.* **2011**, *54*, 5858−5867.
(19) Chartres, J. D.; Busby, M.; Riley, M. J.; Davis, J. J.; Bernhardt, P. V. A Turn-on Fluorescent Iron Complex and its Cellular Uptake. *Inorg. Chem.* **2011**, *50*, 9178−9183.
(20) Duchi, S.; Dambruoso, P.; Martella, E.; Sotgiu, G.; Guerrini, A.; Lucarelli, E.; Pessina, A.; Cocce, V.; Bonomi, A.; Varchi, G. Thiophene-Based Compounds as Fluorescent Tags to Study Mesenchymal Stem Cell Uptake and Release of Taxanes. *Bioconjugate Chem.* **2014**, *25*, 649−655.
(21) Mota, A. A. R.; Carvalho, P. H. P. R.; Guido, B. C.; de Oliveira, H. C. B.; Soares, T. A.; Correa, J. R.; Neto, B. A. D. Bioimaging, Cellular Uptake and Dynamics in Living Cells of a Lipophilic Fluorescent Benzothiadiazole at Low Temperature (4 °C). *Chem. Sci.* **2014**, *5*, 3995−4003.
(22) Crivat, G.; Taraska, J. W. Imaging Proteins Inside Cells with Fluorescent Tags. *Trends Biotechnol.* **2012**, *30*, 8−16.
(23) da Cruz, E. H. G.; Carvalho, P.; Correa, J. R.; Silva, D. A. C.; Diogo, E. B. T.; de Souza, J. D.; Cavalcanti, B. C.; Pessoa, C.; de Oliveira, H. C. B.; Guido, B. C.; da Silva, D. A.; Neto, B. A. D.; da Silva, E. N. Design, Synthesis and Application of Fluorescent 2,1,3-Benzothiadiazole-Triazole-Linked Biologically Active Lapachone Derivatives. *New J. Chem.* **2014**, *38*, 2569−2580.
(24) Mota, A. A. R.; Corrêa, J. R.; Carvalho, P. H. P. R.; de Souza, N. M. P.; de Oliveira, H. C. B.; Gatto, C. C.; da Silva Filho, D. A.; de Oliveira, A. L.; Neto, B. A. D. Synthesis, Structure, Properties, and Bioimaging of a Fluorescent Nitrogen-Linked Bisbenzothiadiazole. *J. Org. Chem.* **2016**, *81*, 2958−2965.
(25) Ravi, M.; Soujanya, T.; Samanta, A.; Radhakrishnan, T. P. Excited-state dipole moments of some Coumarin dyes from a solvatochromic method using the solvent polarity parameter, E^{N}_{T}. *J. Chem. Soc., Faraday Trans.* **1995**, *91*, 2739−2742.
(26) Reichardt, C. Solvatochromic Dyes as Solvent Polarity Indicators. *Chem. Rev.* **1994**, *94*, 2319−2358.
(27) Bortolozzi, R.; Ihmels, H.; Thomas, L.; Tian, M.; Viola, G. 9-(4-Dimethylaminophenyl)benzo[b]quinolizinium: A Near-Infrared Fluorophore for the Multicolor Analysis of Proteins and Nucleic Acids in Living Cells. *Chem. − Eur. J.* **2013**, *19*, 8736−8741.
(28) Li, L. K.; Rola, A-S.; Kaid, F. A.; Ali, A. M.; Alabsi, A. M. Goniothalamin induces cell cycle arrest and apoptosis in H400 human oral squamous cell carcinoma: A Caspase-Dependent Mitochondrial-Mediated Pathway with Downregulation of NF-Kβ. *Arch. Oral Biol.* **2016**, *64*, 28−38.
(29) Choo, C.-Y.; Abdullah, N.; Diederich, M. Cytotoxic Activity and Mechanism of Action of Metabolites from the Goniothalamus Genus. *Phytochem. Rev.* **2014**, *13*, 835−851.
(30) Zhang, Y.; Xiao, F.; Liu, X.; Liu, K.; Zhou, X.; Zhong, C. Cr(VI) induces cytotoxicity in vitro through activation of ROS-mediated endoplasmic reticulum stress and mitochondrial dysfunction via the PI3K/Akt signaling pathway. *Toxicol. In Vitro* **2017**, 232−244.
(31) Chen, X.; Dai, X.; Zou, P.; Chen, W.; Rajamanickam, V.; Feng, C.; Zhuge, W.; Qiu, C.; Ye, Q.; Zhang, X.; Liang, G. Curcuminoid EF24 enhances the anti-tumor activity of Akt inhibitor MK-2206 through ROS-mediated ER stress and mitochondrial dysfunction in gastric cancer. *Br. J. Pharmacol.* **2017**, 1131−1146.
(32) Wu, H.; Liu, S.; Gong, J.; Liu, J.; Zhang, Q.; Leng, X.; Zhang, N.; Li, Y. VCPA, a novel synthetic derivative of α-tocopheryl succinate, sensitizes human gastric cancer to doxorubicin-induced apoptosis via ROS-dependent mitochondrial dysfunction. *Cancer Lett.* **2017**, *393*, 22−32.
(33) Tian, J.; Lu, Z.; Wang, Y.; Zhang, M.; Wang, X.; Tang, X.; Peng, X.; Zeng, H. Nerol triggers mitochondrial dysfunction and disruption via elevation of Ca^{2+} and ROS in Candida albicans. *Int. J. Biochem. Cell Biol.* **2017**, *85*, 114−122.
(34) Tortora, M.; Corsini, S.; Nistri, A. Nicotinic receptors modulate the onset of reactive oxygen species production and mitochondrial dysfunction evoked by glutamate uptake block in the rat hypoglossal nucleus. *Neurosci Lett.* **2017**, *639*, 43−48.
(35) Schneider, C. A.; Rasband, W. S.; Eliceiri, K. W. NIH Image to ImageJ: 25 years of Image Analysis. *Nature Methods* **2012**, *9*, 671−675.

DOI: 10.1021/acsomega.7b00416
ACS Omega 2017, 2, 3774−3784